



HAL
open science

Thermal management design of transformers for Dual Active Bridge power converters

G rard Delette, Ulrich Soupremanien, Serge Loudot

► **To cite this version:**

G rard Delette, Ulrich Soupremanien, Serge Loudot. Thermal management design of transformers for Dual Active Bridge power converters. *IEEE Transactions on Power Electronics*, 2022, 37 (7), pp.8301-09. 10.1109/TPEL.2022.3152692 . cea-03714047

HAL Id: cea-03714047

<https://cea.hal.science/cea-03714047>

Submitted on 5 Jul 2022

HAL is a multi-disciplinary open access archive for the deposit and dissemination of scientific research documents, whether they are published or not. The documents may come from teaching and research institutions in France or abroad, or from public or private research centers.

L'archive ouverte pluridisciplinaire **HAL**, est destin e au d p t et   la diffusion de documents scientifiques de niveau recherche, publi s ou non,  manant des  tablissements d'enseignement et de recherche fran ais ou  trangers, des laboratoires publics ou priv s.

Thermal management design of transformers for Dual Active Bridge power converters

G. Delette, U. Soupremanien, and S. Loudot

Abstract— A methodology for the design of compact transformers operating at high frequency is presented in this paper. A particular emphasis is paid to the thermal management of the magnetic core and of the winding components. For a 7kW Dual Active Bridge DC/DC converter, the objective is to reduce the core volume ($< 80 \text{ cm}^3$), improve the power efficiency ($> 99 \%$) and integrate the serial inductance ($8.7 \mu\text{H}$) as being the leakage inductance of the transformer. A parametric study shows that the heating in the copper winding is very sensitive to the anisotropic thermal conduction behaviour of the wire. Due to this characteristic, a pot-core configuration is prone to a higher warming compared to the E-E core geometry, as the efficiency of the winding cooling is lower. In order to take part of the self-shielding ability of pot-cores, we studied new configurations in which internal thermal drains are inserted into voids specially designed to shorten the distance between the external cooled walls and the hottest points of the winding. The heating of internal components of the transformer and resulting thermo-mechanical stress peak is reduced by 40 % paving the way for robust transformers with a power density that could theoretically reach up to 200 kW/dm^3 .

Index Terms—Design methodology, Transformers, Modeling, Power converter

I. INTRODUCTION

Power converters are increasingly used in a large variety of devices covering power levels ranging from few watts to several hundred of kW [1]. The requirements for stationary applications as well as embedded systems generally involve highly efficient and compact converters. On Board Chargers (OBCs) for electrical vehicles constitute an emblematic case for which a significant downsizing is still expected [2-4]. In this context, the use of Wide Band Gap (WBG) semi-conductors (SiC and GaN) is particularly interesting since WBG transistors allow the switching frequency to be raised, paving the way for passive component miniaturization [5]. In addition, OBCs based on the bidirectional Dual Active Bridge (DAB) topology allow the vehicle batteries to store and deliver power for domestic operation or directly to the grid [6]. In the DAB topology, the transformer plays a crucial role for the galvanic isolation while the serial inductance is devoted to the power

transfer [7]. However, these magnetic components exhibit a large volumetric footprint in the converter and require casing and heat sinks [4, 8-10]. Merging these two distinct magnetic components (serial inductance and transformer) in a single core could contribute to the downsizing. Xue *et al.* [2, 3] designed a compact transformer for a 3.3 kW DC/DC DAB converter operating at 500 kHz for which the leakage inductance, adjusted by the winding configuration, served as the serial inductance. The volume of their magnetic core was 24.5 cm^3 whereas the transformer losses were limited to 20.5 W (efficiency = 99.38 %). Alternatively, Stojadinovic *et al.* [11] showed that the cooling of the passive components could be optimized with a beneficial impact for the converter compactness. Those authors compared several DC/DC DAB converters (50-200 kW) operating at medium frequencies (2-35 kHz) and reported typical values for the volumetric power densities of about 1 kW/dm^3 with air cooling systems. It has been shown that implementing an advanced water-cooling circuit close to the passive components allows increasing the converter power density up to 6 kW/dm^3 [11].

Eventually, the design of the transformer geometry becomes a challenge for achieving simultaneously a high power efficiency, an efficient thermal management and an optimal integration of the electrical functions. Morgorovitch *et al.* [12] developed a design optimization algorithm able to analyze several millions of E-E cores geometries. They showed that analytical models (electrical and thermal) can supply reliable results for a screening purpose, with a very reasonable computation time compared to the one required for a numerical resolution (Finite Element Modelling). A similar analytical approach has been developed for this work including a panel of cooling conditions, winding configurations and core geometries in the screening. The work emphasizes the thermal response of the magnetic core and the winding upon realistic operating conditions and compares different cooling systems. Distinctively from other design approaches [13, 14], a particular attention is paid to the control of temperature gradients and thermo-mechanical stresses arising in the different parts of the transformer. Since ferrite cores are brittle materials, the mechanical robustness should be addressed for the design of compact components. Current and voltage signals

This paragraph of the first footnote will contain the date on which you submitted your paper for review. It will also contain support information, including sponsor and financial support acknowledgment. For example, "This work was supported in part by the U.S. Department of Commerce under Grant BS123456."

G. Delette is with Univ. Grenoble Alpes, CEA, LITEN, DTNM, 38000 Grenoble, France (e-mail: gerard.delette@cea.fr).

U. Soupremanien is with Univ. Grenoble Alpes, CEA, LITEN, DTNM, 38000 Grenoble, France (e-mail: ulrich.soupremanien@cea.fr).

S. Loudot is with Renault, Research division, 1, Avenue du golf 78084, Guyancourt – France (e-mail: serge.loudot@renault.com).

are firstly determined using the electrical model previously developed by Hoang *et al.* [15]. Then, the power losses in the components are computed and injected into the thermal solver as heat sources. The temperature profile inside the transformer is calculated with a nodal approach taking into account the 3D geometry of the component. Finally, a thermo-mechanical analysis is performed by Finite Element in order to determine the thermo-mechanical stresses arising in the selected cores.

II. CONVERTER SPECIFICATIONS

A. Description of the use case

The use case is a compact transformer for a 7kW Dual Active Bridge (DAB) DC/DC (325/360V) power converter for which the leakage inductance of the transformer serves as the serial inductance. Dual Active Bridge insulated converters considered in this work include 2 x 4 switches acting on two symmetrical bridges connected to the primary and secondary sides of a transformer [15]. The turn ratio ($n = N_1/N_2$) of the transformer is adjusted to the output (U_2) and input voltage (U_1). The leakage inductance L_{lk} should be sized to reach the power level for a given phase shift ϕ fixed between primary and secondary voltages.

Following the methodology presented in [15], the values for L_{lk} with an optimal phase shift ϕ and conversion factor $d (= U_2/nU_1)$ are computed in order to (i) minimize the value of current in windings, (ii) fulfil the ZVS (Zero Voltage Switching) mode and (iii) comply with the power level to be delivered. The electrical specifications for the transformer are summarized in Table I.

TABLE I
ELECTRICAL SPECIFICATIONS FOR THE TRANSFORMER

Converter operating parameters	Values
Power P	7 kW
Switching frequency f	100 kHz
Primary voltage U_1	325 V
Secondary voltage U_2	360 V
Primary current (rms) I_1	23 A
Phase shift ϕ	21.6 °
Turn ratio n	1
Leakage inductance L_{lk}	8.7 μ H

B. Additional constraints

The selected magnetic material is the N87 ferrite grade from TDK that is suited for an operation at 100 kHz. Distinct primary and secondary coils are stacked in the core in order to create the flux leakage and to adjust the inductance to the prescribed level.

The maximal volume and minimal transformer efficiency target values are respectively 80 cm³ and 99 %.

III. MODEL DESCRIPTION

A. Power loss model

The power loss (copper and core) in the transformers is calculated with dedicated existing models for which the current and voltage values of Table I are the input parameters. The first contribution to power loss comes from the core material and is given by the Steinmetz's model:

$$P_{Fe} = K \times f^\alpha \times B^\beta \times V_{Fe} \quad (1)$$

In (1) α , β and K are material parameters established for a given core grade, f denotes the switching frequency, B the amplitude of induction and V_{Fe} the core volume. Considering the square-wave form of the voltage signal, the induction peak to be considered in (1) is given by [15] as:

$$B = \frac{U_1}{4A_c f N_1} \quad (2)$$

where A_c is the magnetic cross section of the core and N_1 the turns number of the primary winding.

Copper winding dissipation by Joule effect is determined according to the analytical approach of Tourkhani *et al.* [16] established for Litz wires. With the known root mean square (rms) values of the current I at primary (subscript 1) and secondary (subscript 2) sides, the dissipated power is calculated as:

$$P_{Cu} = R_{AC,1} \times I_1^2 + R_{AC,2} \times I_2^2 \quad (3)$$

Skin and proximity effects are accounted in the following expression of the AC resistance of the winding:

$$R_{AC} = R_{DC} x [\Psi(x) - N_s C_s \Phi(x)] \quad (4)$$

In (4) x , a variable to be optimized, denotes the diameter of the strand d_s normalized to the skin depth $\delta = 0.075/\sqrt{f}$ and N_s accounts for the number of strands in a wire section.

The functions $\Psi(x)$ and $\Phi(x)$ are combinations of Bessel functions and can be approximated by the first terms of their Taylors expansion, providing that x values remain small ($x < 1$):

$$\Psi(x) = \frac{1}{x} + \frac{1}{3.2^8} x^3 - \frac{1}{3.2^{14}} x^5 + \dots \quad (5)$$

$$\Phi(x) = -\frac{1}{27} x^3 - \frac{1}{2^{14}} x^7 + \dots \quad (5')$$

The parameter C_s in (4) is expressed as:

$$C_s = \frac{\pi^2 k_s}{24} \left(16m^2 - 1 + \frac{24}{\pi^2} \right) \quad (6)$$

In (6) m is the number of the layers in the lateral direction required for adjusting the winding within the coil window and k_s is the packing factor of strands within a section of Litz wire. Instead of considering a fixed number of strands N_s , we assume here that the diameter of Litz wire d_w is a known parameter, determined in a previous step of the transformer design. N_s is then linked to the optimization variable x according to the geometrical relation: $N_s = k_s d_w^2 / d_s^2 = k_s d_w^2 / \delta^2 x^2$.

Finally, the expression of R_{AC} becomes:

$$R_{AC} = R_{DC} x \left[\Psi(x) - \frac{k_s d_w^2 C_s}{\delta^2 x^2} \Phi(x) \right] \quad (7)$$

For an optimization purpose, the minimum value of the normalized resistance $R_{AC}/[R_{DC}x]$ is sought instead of the smallest R_{AC}/R_{DC} value [16]. Actually, low strand diameters (d_s ,

$\ll \delta$) would theoretically lead to minimize the Litz wire AC resistance since $R_{AC} \rightarrow R_{DC}$, but such wire are not economically viable for high frequencies. The minimum of the ratio $R_{AC}/[R_{DC}x]$ is reached for a strand diameter given by:

$$d_{s,opt} \sim \frac{32\sqrt{3}\delta^2}{\pi k_s d_w \sqrt{16m^2 - 1 + 24/\pi^2}} \sim \frac{8\sqrt{3}\delta^2}{\pi k_s d_w m} \quad (8)$$

The AC resistance is equal to $2 \times R_{DC}$, as found in [16]. It is worth noting that the optimal value of the individual strand diameter decreases linearly with the square of the skin depth δ^2 (i.e. with the switching frequency) and also decreases linearly with the width of the coil windows ($\sim d_w m$).

For practical applications, the minimal strand diameter will be, however, limited to $32 \mu\text{m}$ involving that for cases where $d_{s,opt}$ is found to be lower, the R_{AC} will be not be minimized and remain higher than $2 \times R_{DC}$.

The previous formalism (4-8) stands for a sinusoidal current. Taking into account the actual signal $i(t)$ given by the electrical model, we used the equivalent frequency expression derived by Sullivan [17] in the skin and proximity effects calculation:

$$f_{eq} = \frac{1}{2\pi} \sqrt{\frac{\int_0^{2\pi} \left| \frac{di}{dt} \right|^2 dt}{\int_0^{2\pi} |i|^2 dt}} \quad (9)$$

B. Thermal model

Thermal behaviour of transformers has been widely depicted by Finite Element Analysis or by thermal resistance networks either in steady or transient states [12,18,19]. The heat generated within the transformer is dissipated to the surrounded environment by conduction through the solid parts of the core toward the transformer external surface. In the model, heat conduction in the bulk is accounted by the Fourier's laws whereas thermal flux on external surfaces are calculated with heat transfer coefficients.

On the core surface, cooling may occur via different thermal exchange modes, namely free convection, forced convection, radiation, fixed wall temperature (heat sink) or may be impeded if adiabatic conditions prevail. These boundary conditions are sometimes combined or distributed on the different portions of the external surface as in the previous work of Bakri *et al.* [18].

The assumption of a steady state regime established within the core constitutes a reasonable simplification to compare the ability of different transformer designs to operate over long periods at moderate temperatures. However, the stationary problem cannot be analytically solved due to the 3D geometry complexity and some non-linearities that appear in heat transfer correlations (for instance radiative heat transfer coefficients depend on the temperature). Nodal numerical schemes, or lumped models, based on the representation of the transformer by a network of thermal resistances have been widely used to solve this kind of problems with low computational costs [12]. The magnetic core as well as the winding (taken here as an equivalent solid medium) are discretised into regular sub-parts forming a 3D meshing. Geometrical points (nodes) for which the temperature is solved are positioned at the centre of the

mesh elements.

Two adjacent nodes are connected through a thermal resistance that accounts for the material properties encountered along the heat flow path. In a 3D approach, each node can be connected up to six surrounding nodes within the solid. The general expression of the thermal resistance between two nodes is given by the classical formula [19]:

$$R_{th} = \sum_{i=1}^n \frac{l_i}{\lambda_i S_i} \quad (10)$$

In (10) the summation is performed over the n subdivisions of the path that links the couple of nodes. Each subdivision of the length l_i should exhibit a constant cross-section S_i normal to the path and a uniform thermal conductivity (λ_i). The thermal conductivity values of materials used in the model are indicated in Table II.

Besides the volumetric nodes, surface nodes are added at the centre of the squared surface elements intersecting the external surface to take into account the local boundary conditions. Finally, heat source terms (derived from the average power loss density derived from (1) and (3) $Q_{Fe} = P_{Fe}/V_{Fe}$ or $Q_{Cu} = P_{Cu}/V_{Cu}$) are applied at the central node of the corresponding volumetric elements.

TABLE II
THERMAL CONDUCTIVITY VALUES USED FOR THE MATERIALS

Materials	Values in W.m ⁻¹ .K ⁻¹
Ferrite core (MnZn)	4 [18]
Copper	380 [18]
Insulating (epoxy resin)	1.2 [20]
Thermal drain (AlN)	60 [21]
Coil former	1 (estimated)

For a given node labelled k , belonging to a cubic element of volume V_k , the combination of the flux conservation rule and the heat transfer laws leads, after rearrangement, to a linear equation of the general form [18]:

$$\sum_{l=1}^n \frac{T_k - T_l}{R_{th}^{kl}} = Q_{Fe \text{ or } Cu} \times V_k \quad (11)$$

For the nodes located on the surface, linearized heat transfer relations (using fixed external temperature values) complete the linear system of equations. In the case of a radiative transfer mode, an iterative procedure is implemented (relaxation scheme) to obtain the convergence of the temperature values on the surface nodes.

It is worth noting that (10-11) account also for non-isotropic conduction by allowing different conductivity values in each direction. This feature is implemented for describing the winding anisotropic behaviour. Several studies [20,22] shown that the thermal conductivity should be lower in directions perpendicular of the wire packing (transverse), due to the effects of electrical insulators, than the value experienced along the wire (longitudinal). In the transverse direction, the effective thermal conductivity of the winding is computed considering a periodic arrangement of thermal barriers, each associated to one

constitutive medium of the winding, i.e. with a conductivity equal to λ_{Cu} for the copper and λ_g for the insulator. In the longitudinal direction, the thermal barriers are taken as being in parallel. Materials thermal conductivity values are given in Table II.

Fig. 1 focuses on the distribution of the thermal resistances $R_{th}^{w,\perp}$ and $R_{th}^{w,\parallel}$ applied in three winding elements surrounding a corner of the ferrite core in the mid-plane ($z = 0$). Furthermore, specific thermal resistances are added at the interfaces between winding and ferrite elements to account for the thermal barrier effect created by coil former and insulating layers. It is worth noting that these last two media are not explicitly described in the geometrical model used in the following sections. However, two values of interfacial thermal resistance are ascribed: (i) at the interfaces between the inner ferrite column and winding $R_{th}^{w,int}$ where an actual contact via the coil former exists and (ii) at the interfaces between the external windings' envelop and the inner part of the external ferrite legs $R_{th}^{w,ext}$ for which the contact may be less effective.

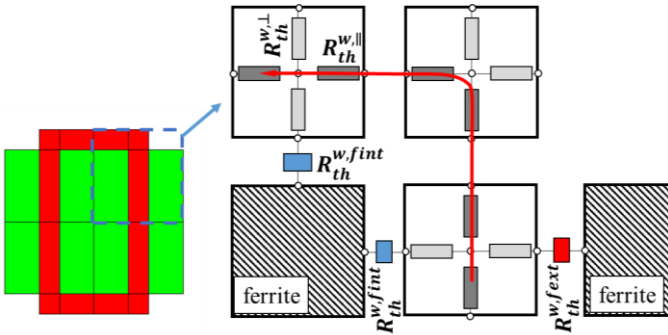


Fig. 1. Schematic representation of the thermal model in the mid-plane ($z = 0$) with a close-up view at the corner of the transformer. Only thermal resistances in the copper winding (dark grey: high conductivity in the wire direction) and at the interface with the core are indicated for highlighting the anisotropic characteristics. The red arrow shows the current direction.

C. Geometrical constraints for the transformer core design

Assuming that the primary and secondary windings are axially separated and each one positioned on a half part of the central leg of the core along the z axis, the leakage inductance L_{lk} can be related to the core geometry via the following expression [15]:

$$L_{lk} = \frac{1}{3} \mu_0 N_1^2 MLT \frac{h}{b} \quad (12)$$

MLT denotes the mean-length of wire per turn, h and b define the rectangular winding window height and width.

Eq. (12) constitutes a geometrical constraint to be fulfilled to obtain a leakage inductance value equal to the one prescribed by the electrical model.

Two other geometrical constraints involve the magnetic cross section A_c and the winding window area A_w : if we assume that both a maximal induction B_{max} and a maximal current density J_{max} values are allowed during the operation of the transformer, the areas can be minimized as following:

$$A_c = \frac{U_1}{4B_{max}fN_1} \quad \text{and} \quad A_w = \frac{2N_1I_1}{k_fJ_{max}} \quad (13)$$

Combining these two last relations gives rise to the well-known areas product rule for transformer design. However, the implementation of this approach needs to define, a priori, some values for B_{max} and J_{max} . Consequently, this method would lead to an over-estimation of the transformer volume if too large margins were considered [17]. In this work, it has been preferred to deal directly with the impact of the induction and current density on the thermal response of the transformer, a reasonable heating of components being the actual constraints for the design. Practically, the maximal temperature in the magnetic core has been limited to 130°C whereas the temperature in the winding should always remained below 180°C (class H insulation). This temperature limitation, suited for the selected materials, involves specific geometrical constraints that cannot be simply expressed in the general case via analytical relations like (13). Thus, the fulfilment of the thermal constraint can only be validated after a thermal analysis being performed on the pre-determined geometry.

In order to carry out the optimization, we systemically test all physically acceptable values for B_{max} and J_{max} . For the current density J_{max} the screening range is [3-15 A/mm²] whereas candidate values for B_{max} are determined from the Steinmetz model, in order to verify that the specific core loss lies within [300-1500 W/m³].

Elsewhere, the magnetizing inductance of the core L_{mag} should be larger than L_{lk} ($L_{mag} > 50-100 L_{lk}$) in order to maximise the utilisation factor of the transformer [8]. Again, this condition introduces a geometrical restriction since L_{mag} depends on the magnetic cross section A_c and on the magnetic length l_m of the core:

$$L_{mag} = \mu_0 \mu_r N_1^2 \frac{A_c}{l_m} \quad (14)$$

Finally, three other constraints have been added for completing the core design: a minimal value for the transformer power efficiency (η_{min}), a maximal volume allowed for the core and winding (V_{max}) and a maximal number of strands in the Litz wire ($N_{s,max}$).

D. Numerical implementation

Fig. 2 illustrates two typical 3D transformer geometries (E-E and pot-core) considered in this study. Each geometry is depicted via four geometrical parameters (a, b, d, h).

The screening of the transformers configurations is monitored by a custom software developed on the Scilab 6.0.2 open source platform. After selecting the materials, the core type and the allowed boundary conditions in a database, the exploration of a four-dimensional domain covering a wide range of configurations is performed. Each configuration belonging to the domain is determined by a set of four coordinates: the allowed induction B_{max} , the current density J_{max} and two independent geometrical parameters (a and d). For each point of a grid that discretizes the domain, (12-14) are solved in order to determine the three last geometrical parameters (N_1, b, h) that fully define the transformer. The

thermal analysis is then performed and if all the design constraints are fulfilled, the parameters are saved before going on to the next point of the grid. Once completed, the results of the screening are post-processed in order to supply performance maps displaying the volume, efficiency and heating of all the possible configurations. Finally, thermo-elastic stresses in the core are computed for selected configurations with a Finite Element solver (Cast3M [23]) with the following values for the ferrite materials: Young's modulus = 150 GPa, Poisson ratio = 0.3 and coefficient of thermal expansion = $1.2 \cdot 10^{-5}$ 1/K [24].

Fig. 3 compares the CPU computational cost (PC Core I5) for different mesh refinements of an E-E core considering cooling by radiative transfer and forced convection. The convergence on the temperatures in core and winding is observed when the number of 3D elements reaches 512 (with unrealistic values regarding material limitation but selected to exacerbate the non-linear radiative component). This corresponds to a meshing of the transformer with four elements in each direction of the different legs (Fig. 4a). This mesh refinement has been adopted in the following.

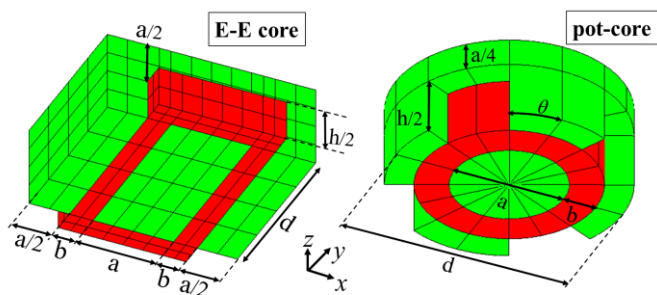


Fig. 2. 3D representations of core geometries with the parametrization considered in the study (half part represented for each case, red: winding, green: ferrite core). In order to respect a constant magnetic section the opening angle in the pot-core geometry is given as $\theta = \pi a^2 / (4[d^2 - (a + 2b)^2])$.

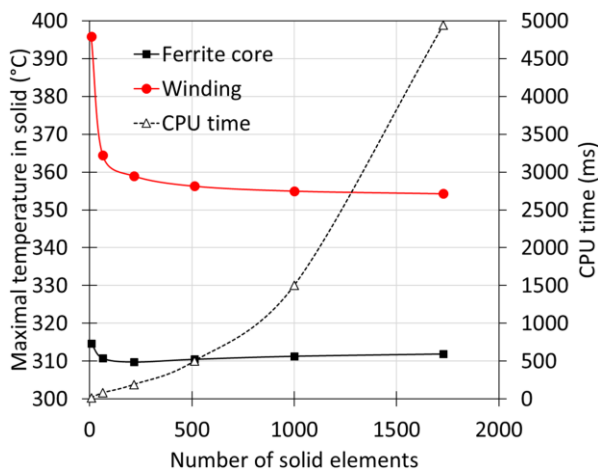


Fig. 3. Dependence of the thermal analysis results and CPU time on the geometrical mesh refinement for the case of a E-E core with radiative and forced convection conditions ($a = 16.8$ mm, $b = 4.9$ mm, $h = 16.8$ mm, $d = 34.9$ mm, $P_{Fe} = 29$ W, $P_{Cu} = 105$ W, $h = 100$ W/m²/K, $T_{ext} = 25^\circ\text{C}$).

Fig. 4 shows the temperature maps obtained with the thermal resistance network (this work) and with the Finite Element software Cast3M, for the same conditions. A high value of winding loss (207 W, non realistic) has been arbitrarily chosen in order to exacerbate the thermal gradients. Both approaches

reveal that the heat flow is channelled along the wire direction due to the large conductivity of copper whereas the cooling in the two other directions is much less efficient. The temperature profiles along the main axis are compared in the Fig. 5 and found to be in good agreement. This last result confirms that the thermal gradients are correctly computed in the present study with the nodal approach.

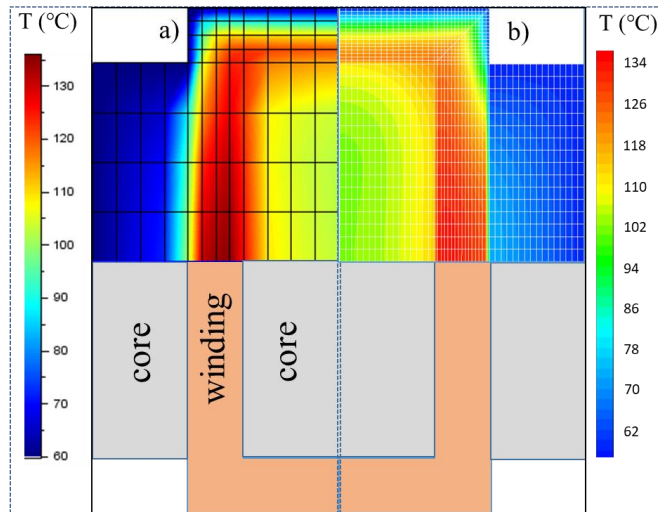


Fig. 4. Comparison between the temperature distribution calculated in the mid-plane ($z = 0$) of an E-E core (fixed temperature on external surfaces to 60°C) with the nodal approach of the present study a) and with Cast3m F.E software b). Only a quarter part of the transformer is mapped due to symmetries, ($a = 16.8$ mm, $b = 4.9$ mm, $h = 16.8$ mm, $d = 34.9$ mm, $P_{Fe} = 29$ W, $P_{Cu} = 207$ W). Note that colour graduations from the two different numerical tools exhibit slight differences.

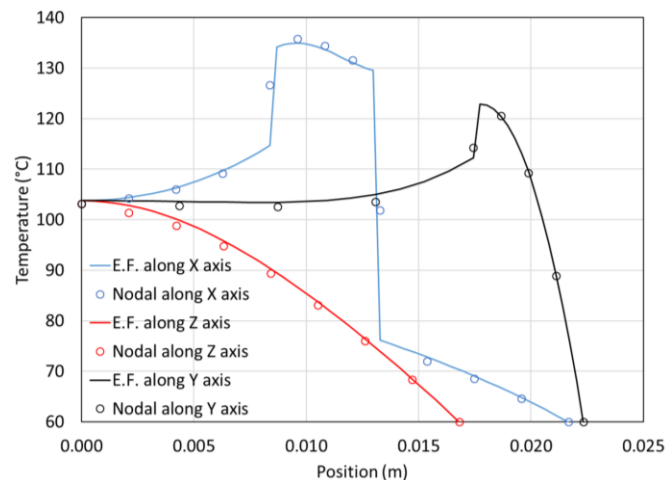


Fig. 5. Comparison of the temperature profiles in the main axis of an E-E core obtained with the nodal approach of this study (dots) and with the F.E software Cast3m (solid lines). The position are taken from the central point. Conditions corresponding to the case depicted on Fig. 4.

IV. ANALYSIS OF THE E-E CORE GEOMETRY

Two different cooling configurations are compared in the following paragraphs:

- (i) the air-convection case, i.e. a forced convection mode with an heat exchange coefficient of 100 W/m²/K, $T_{ext} = 25^\circ\text{C}$, applied on all external surfaces (core + winding),
- (ii) the terminal cold plates case, i.e. a combination of

a fixed temperature (60°C) applied on the upper and lower plane surfaces of the transformer (cold plates) and a free convection mode ($h_{ex} = 5 \text{ W/m}^2/\text{K}$, $T_{ext} = 25^\circ\text{C} + \text{radiation}$) as boundary conditions for all other external surfaces. This cooling is costly due to the implementation of a refrigerant circuit.

A. Performances of E-E cores with forced convection

The performance map on Fig. 6 displays all the transformers that fulfil the optimization constraints with the air-cooling case (forced convection). Each solution is represented by a coloured dot plotted in a 2D diagram drawn with the volume and the power efficiency as the main axes. The colour of each dot is indicative of the maximal temperature reached in the ferrite core under operation.

Fig. 6 shows that for a given transformer efficiency the core temperature decreases when the transformer volume rises. This comes from the larger external surface that enhances the thermal exchange by convection. The region of the diagram with the lowest volumes ($< 60 \text{ cm}^3$) is actually bounded by two limiting curves: the first one corresponds to the maximum allowable temperature of the core (130°C). The second arises with the maximal geometrical packing factor (0.78) allowable for the wire in the winding area.

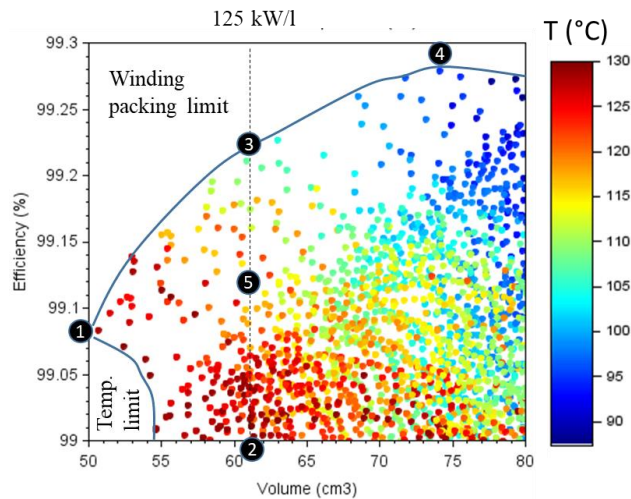


Fig. 6. Performance map for E-E transformers (requirements of Table I), cooling via forced convection ($h = 100 \text{ W/m}^2/\text{K}$, $T_{ext} = 25^\circ\text{C}$).

The minimal core volume is about 50 cm^3 and corresponds to the crossing of the two limiting curves. In order to illustrate this finding, Table III details five particular transformer configurations identified by labels positioned at some extremal zones of this map (#1-5).

The comparison of solutions #2, #3 and #5 with the same volume ($\sim 60 \text{ cm}^3$) shows that an elongated central leg (characterized by a high value of the ratio $K_l = d/a$) is beneficial regarding the core loss. The best solution #3 allows a larger magnetic section for the given volume with a limited rise in the winding length (MLT). Consequently, the magnetic induction and the core loss are lower in the solution #3. The copper loss remains steady along this constant volume line until the geometrical packing factor of the wire in the winding area

reaches the maximum value ($\pi/4$).

Similarly, the points #1 and #4 correspond to the asymptotic, lower values of the total losses for transformers exhibiting total volumes equal respectively to 50 and 74 cm^3 . It is worth noting that the mechanical stresses (Von Mises) decrease with the power loss. In the case #4, the maximal stress is 38 MPa for 50 W. The maximal stress is located near the internal edges of the core as evidenced by M. de Graaf *et al.* [25] who also calculated thermo-mechanical stresses in E-E ferrite cores. These authors found stress values of about 4 MPa but, in their study, the power loss and core heating were lower (resp. 3W and 15°C), i.e. one order of magnitude under the current values. M. de Graaf *et al.* concluded that “*fracture of the core under normal operating conditions is very unlikely*” [25]. Considering the rise in power loss and heating found here for compact transformers, the mechanical reliability of inductive cores should be re-assessed.

TABLE III
DETAILS OF TRANSFORMER CONFIGURATIONS (E-E CORES, AIR COOLING)
CORRESPONDING TO THE FIVE SOLUTIONS LABELLED ON FIG. 6

Transformer characteristics	#1	#2	#3	#4	#5
Total volume (cm^3)	50.6	61.1	60.8	74.1	61.3
Efficiency (%)	99.08	99	99.21	99.28	99.12
Width a (mm)	10.3	22.5	13.5	18.2	18.2
Depth d (mm)	38.0	18.5	35.4	31.3	24.8
Width b (mm)	10.4	9.7	10.4	10.5	9.9
Height h (mm)	19.1	20.4	19.0	18.9	20.0
Aspect ratio $K_l = d/a$	3.7	0.8	2.6	1.7	1.4
Nb. of turns ($N_1 = N_2$)	9	9	9	9	9
Core loss (W)	33.5	39.4	24.6	19.8	30.9
Copper loss (W)	30.6	30.5	30.6	30.6	30.6
Section A_c (mm^2)	391.1	415.9	478.9	569.7	450.5
Area A_w (mm^2)	140.7	142.8	140.4	140.3	142.2
MLT (mm)	139.2	121.8	140.7	142.0	126.5
Nb. of strands N_s	1177	910	1201	1222	978
Strand diam. (μm)	50	53	49	49	52
Wire packing factor	0.77	0.66	0.77	0.78	0.69
Core temp. ($^\circ\text{C}$)	129	122	108	95	115
Winding temp. ($^\circ\text{C}$)	126	120	110	99	116
Max. stress (MPa)	51	55	43	38	45

B. Performances of E-E cores with terminal cold plates

The performance map for this cooling configuration is drawn on Fig. 7. Five particular solutions are labelled (#1-5) on Fig. 7 with details on the transformer geometries given on Table IV. The transformer with the minimal volume (#1, 43 cm^3) is about 12% more compact compared to the optimal configuration obtained with the forced convection regulation. The same limitation regarding the geometrical packing factor of the winding, already noticed with forced convection, arises (points #1, 3 and 4). However, in this case, the correlation between the core heating and the volume is not straightforward. When cold plates are used, the increase in the geometrical factor K_l leads to a better cooling of the core and the winding, as pointed by the combination of data plotted on Figs. 7 and 8. This comes from larger areas of the transformer in contact with the thermally regulated plates obtained with higher K_l values (see the comparison of points #2 and #5). It is worth noting that the lower heating and the lower mechanical stresses are achieved for the case #5 with the highest K_l value (9.5).

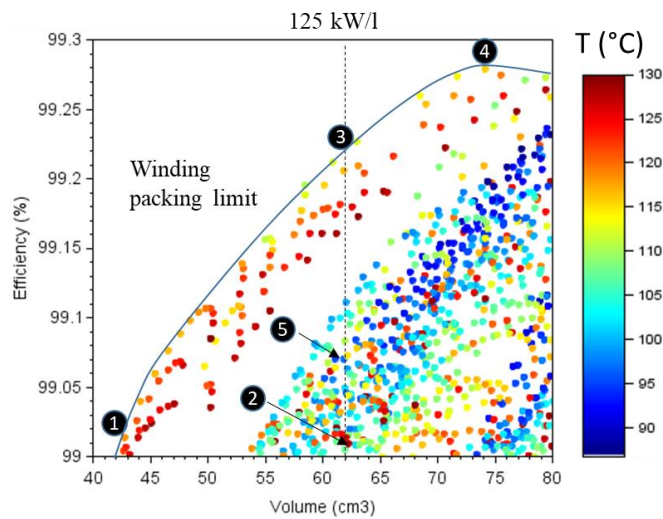


Fig. 7. Performance map for E-E transformers (requirements of Table II), cooling via fixed temperature on upper and lower surfaces (cold plates, $T_{ext} = 60^\circ\text{C}$).

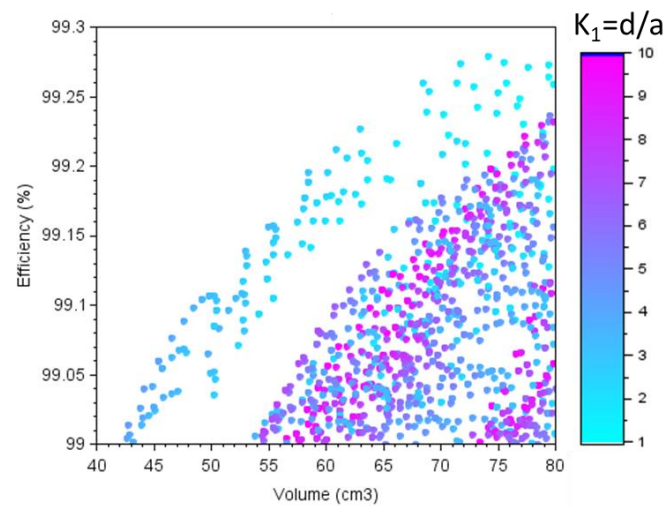


Fig. 8. Geometrical aspect ratio $K_1=d/a$ corresponding to the performance map of Fig. 7.

TABLE IV
DETAILS OF TRANSFORMER CONFIGURATIONS (E-E CORES,) CORRESPONDING TO THE FIVE SOLUTIONS LABELLED ON FIG. 8

Transformer characteristics	#1	#2	#3	#4	#5
Total volume (cm^3)	42.7	62.2	62.9	74.1	62.8
Efficiency (%)	99.01	99.01	99.23	99.28	99.08
Width a (mm)	9.2	13.9	14.2	18.2	8.8
Depth d (mm)	42.3	43.9	34.8	31.3	83.6
Width b (mm)	9.2	7.9	10.4	10.5	6.1
Height h (mm)	16.7	17.3	19.0	18.9	16.8
Aspect ratio $K_1 = d/a$	4.6	3.2	2.4	1.7	9.5
Nb. of turns ($N_1 = N_2$)	9	8	9	9	6
Core loss (W)	29.9	20.1	23.5	19.8	25.8
Copper loss (W)	39.1	49.2	30.6	30.6	38.3
Section A_c (mm^2)	389.3	608.8	494.8	569.7	739.3
Area A_w (mm^2)	109.2	99.1	140.4	140.3	75.8
MLT (mm)	140.8	147.9	140.8	142.0	210.0
Nb. of strands N_s	742	413	1203	1224	353
Strand diam. (μm)	56	64	49	49	81
Wire packing factor	0.78	0.56	0.77	0.78	0.74
Core temp. ($^\circ\text{C}$)	119	129	113	116	96
Winding temp. ($^\circ\text{C}$)	134	155	126	132	107
Max. stress (MPa)	49	65	46	53	32

V. ANALYSIS OF THE POT CORE GEOMETRY

The self-shielding ability constitutes the main advantage of pot-core transformers regarding the electromagnetic compatibility. However, in this geometry, the evacuation of the heat from the copper conductor in the radial direction is hindered by the large area of the curved ferrite legs that covers the winding outer surface. In this part, the improvement of the thermal management performed via two cold plates is investigated for this geometry.

A. Performances of pot-cores with terminal cold plates

Five solutions (#1-5) are labelled on the performance map corresponding to this geometry (Fig. 9) with geometrical details summarized in Table V.

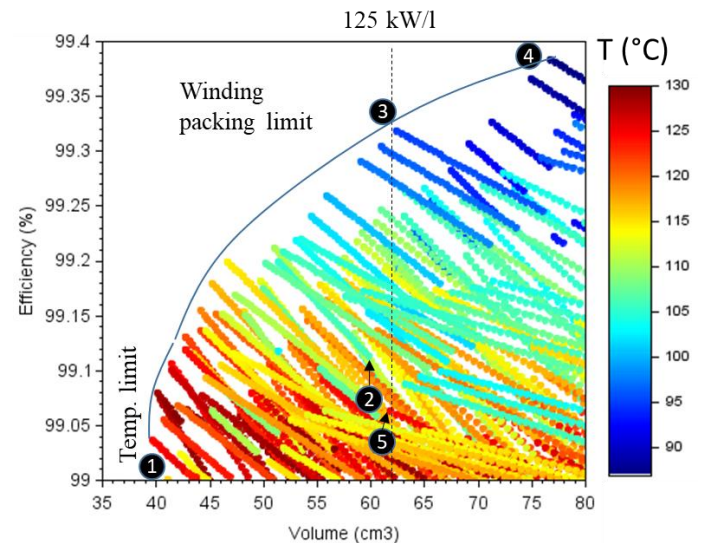


Fig. 9. Performance map for pot-core transformers (requirements of Table II), cooling via fixed temperature on upper and lower surfaces (cold plates, $T_{ext} = 60^\circ\text{C}$).

The volume of the most compact transformer (case #1) is about 40 cm^3 , i.e. 10% less than the equivalent E-E core. This is due to fact that the axisymmetric pot-core allows larger winding areas and lower length per turn (resp. 118 mm^2 and 85 mm for a total volume of 40 cm^3) compared to the E-E core (resp. 108 mm^2 and 141 mm for a total volume of 43 cm^3). Consequently, it is possible to raise the winding turn number up to 12 (vs 9 for E-E) and then to reduce the induction and core loss. As for E-E cores, the performance is driven by the increase in the magnetic section providing that the area of the windows winding remains acceptable. A limitation comes from the winding packing factor but also, for pot-cores, from the maximal allowable value of the opening angle for the external legs (45° , see cases #3 and #4).

Configurations #2, #5 are located in the same region of the performance map (vol. $\sim 62 \text{ cm}^3$, efficiency $\sim 99.1\%$) but exhibit different heating and mechanical stress values. Case #2 is a more favourable configuration with a high aspect ratio ($K_1 = 2.8$) which allows wide terminal plates, less heating and a stress reduced by a factor 2 compared to the case #5. The mechanical stress for the most compact pot core (#1) is found

to be greater (100 MPa) than in its E-E counterpart (50 MPa), and also greater than the mechanical strength of the ferrite material (90 MPa [24]). For this reason, the reduction of the thermal gradients in this geometry is investigated in the next section.

TABLE V
DETAILS OF TRANSFORMER CONFIGURATIONS (POT-CORES, COLD PLATES)
CORRESPONDING TO THE FIVE SOLUTIONS LABELLED ON FIG. 9

Transformer characteristics	#1	#2	#3	#4	#5
Total volume (cm ³)	39.6	61.8	62.4	77.1	62.3
Efficiency (%)	99.04	99.14	99.32	99.38	99.06
Width a (mm)	21.1	19.6	23.2	22.9	27.2
Depth d (mm)	46.3	55.5	55.3	60.2	54.9
Width b (mm)	9.9	15.2	13.4	16.2	6.9
Height h (mm)	16.9	24.3	18.1	19.7	22.8
Opening angle (deg)	42.5	29.7	43.9	41.1	25.1
Aspect ratio $K_1 = d/a$	2.2	2.8	2.4	2.6	2.0
Nb. of turns ($N_1 = N_2$)	12	12	12	12	9
Core loss (W)	19.2	37.8	16.7	20.9	18.5
Copper loss (W)	48.2	22.3	31.1	22.4	47.3
Section A_c (mm ²)	349.0	303.0	424.2	411.2	581.1
Area A_w (mm ²)	118.2	257.6	181.7	252.7	92.6
MLT (mm)	84.9	90.3	98.2	102.3	98.5
Nb. of strands N_s	558	2872	1766	3653	253
Strand diam. (μm)	52	35	39	33	72
Wire packing factor	0.63	0.68	0.75	0.78	0.52
Core temp. ($^{\circ}\text{C}$)	125	102	95	87	125
Winding temp. ($^{\circ}\text{C}$)	160	104	110	93	164
Max. stress (MPa)	99	47	44	37	121

B. Improvement of the thermal dissipation in pot-cores

As a general trend, the thermal management should be more efficient when both the core and the winding elements are directly cooled. The pot-core component could barely reach this purpose without a modification of its basic geometry since, due to external curved legs, the winding could not directly be in contact with external heat sink.

Fig. 10 shows how the previous compact configuration #1 could be improved by the insertion of high thermal conductivity material (AlN [21]) adjusted to fill the empty regions of the ferrite core. Four trapezoidal holes could be designed in the upper and lower circular plates and filled with AlN in order to create connections between the cold plates and the winding (Fig. 10). These four voids in the ferrite core are small enough to avoid a reduction of the magnetic section. Taking advantage of the good conductivity of the AlN material, the temperature in the winding can be lowered by 40 $^{\circ}\text{C}$. This would mitigate the wire degradation risk without any volume penalty. The temperature elevation in the core is reduced by 50% leading to a decrease of 40% in the thermos-mechanical stress (65 MPa) which is then lower than the bending strength. This result emphasizes how some geometrical details could favour the thermal management of the transformer. Such refinement (such thin walls and voids) could be obtained considering recent progress in manufacturing process of sintered ferrite components like the Powder Injection Moulding previously investigated by some of the authors [26].

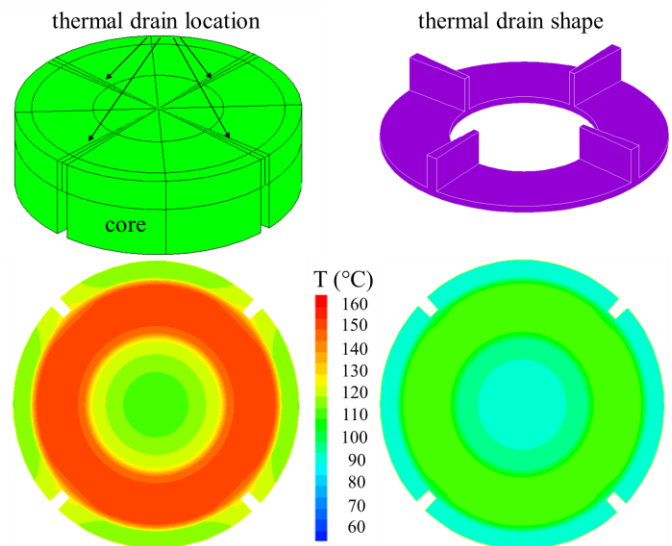


Fig. 10. Temperature distribution calculated in the mid-plane ($z = 0$, cold plates) of the pot-core solution #1 (left), temperature distribution after insertion of thermal drains (right) as represented in the 3D views (up) of the core (green) and drains (magenta) of a half part of the transformer.

VI. CONCLUSION

The thermomechanical analysis of compact magnetic passive components, taking into account realistic operating conditions, shed the light on thermo-mechanical stresses that could lead to a limitation in the downsizing when ferrite materials are used. Closed pot-core structures with self-shielding ability are more prone to heating and to developing thermal gradients than the E-E geometry. In order to mitigate the failure risk in this configuration, thermal management could be improved by inserting high thermal conductive materials close to the winding in order to dissipate the power loss.

ACKNOWLEDGMENT

The authors would like to thank the "Institut CARNOT Energies du Futur" for its support.

REFERENCES

- [1] B. Zhao, Q. Song, W. Liu and Y. Sun, "Overview of Dual-Active-Bridge Isolated Bidirectional DC-DC Converter for High-Frequency-Link Power-Conversion System," in *IEEE Transactions on Power Electronics*, vol. 29, no. 8, pp. 4091-4106, Aug. 2014, doi: 10.1109/TPEL.2013.2289913.
- [2] L. Xue et al., "Bi-directional PHEV battery charger based on normally-off GaN-on-Si multi-chip module," in *2014 IEEE Applied Power Electronics Conference and Exposition - APEC 2014*, Fort Worth, TX, 2014, pp. 1662-1668, doi: 10.1109/APEC.2014.6803529.
- [3] L. Xue, M. Mu, D. Boroyevich and P. Mattavelli, "The optimal design of GaN-based Dual Active Bridge for bi-directional Plug-IN Hybrid Electric Vehicle (PHEV) charger," in *2015 IEEE Applied Power Electronics Conference and Exposition (APEC)*, Charlotte, NC, 2015, pp. 602-608, doi: 10.1109/APEC.2015.7104411.
- [4] F. Krismer and J. W. Kolar, "Efficiency-Optimized High-Current Dual Active Bridge Converter for Automotive Applications," in *IEEE Transactions on Industrial Electronics*, vol. 59, no. 7, pp. 2745-2760, July 2012, doi: 10.1109/TIE.2011.2112312.
- [5] S. Inoue and H. Akagi, "A Bidirectional Isolated DC-DC Converter as a Core Circuit of the Next-Generation Medium-Voltage Power Conversion System," in *IEEE Transactions on Power Electronics*, vol. 22, no. 2, pp. 535-542, March 2007, doi: 10.1109/TPEL.2006.889939.
- [6] G. Oggier, G. O. García and A. R. Oliva, "Modulation strategy to operate the dual active bridge DC-DC converter under soft switching in the whole

- operating range," in *IEEE Transactions on Power Electronics*, vol. 26, no. 4, pp. 1228-1236, April 2011, doi: 10.1109/TPEL.2010.2072966.
- [7] J. Schmenger, S. Endres, S. Zeltner and M. März, "A 22 kW on-board charger for automotive applications based on a modular design," in *2014 IEEE Conference on Energy Conversion (CENCON)*, Johor Bahru, 2014, pp. 1-6, doi: 10.1109/CENCON.2014.6967467.
- [8] M. N. Kheraluwala, R. W. Gascoigne, D. M. Divan and E. D. Baumann, "Performance characterization of a high-power dual active bridge DC-to-DC converter," in *IEEE Transactions on Industry Applications*, vol. 28, no. 6, pp. 1294-1301, Nov.-Dec. 1992, doi: 10.1109/28.175280.
- [9] H. van Hoek, M. Neubert, A. Kroeber and R. W. De Doncker, "Comparison of a single-phase and a three-phase dual active bridge with low-voltage, high-current output," in *2012 International Conference on Renewable Energy Research and Applications (ICRERA)*, Nagasaki, 2012, pp. 1-6, doi: 10.1109/ICRERA.2012.6477466..
- [10] H. van Hoek, M. Neubert and R. W. De Doncker, "Enhanced Modulation Strategy for a Three-Phase Dual Active Bridge—Boosting Efficiency of an Electric Vehicle Converter," in *IEEE Transactions on Power Electronics*, vol. 28, no. 12, pp. 5499-5507, Dec. 2013, doi: 10.1109/TPEL.2013.2251905..
- [11] M. Stojadinović and J. Biela, "Modeling and Design of a Medium-Frequency Transformer for High-Power DC-DC Converters," *IEEE Journal of Industry Applications*, vol. 8, no. 4, pp. 685-693, 2019.
- [12] M. Mogorovic and D. Dujic, "Thermal modeling and experimental verification of an air cooled medium frequency transformer," in *2017 19th European Conference on Power Electronics and Applications (EPE'17 ECCE Europe)*, Warsaw, 2017, pp. P.1-P.9, doi: 10.23919/EPE17ECCEEurope.2017.8099176.
- [13] R. Kondo, P. Schülting, A. H. Wienhausen and R. W. De Doncker, "An Automated Component-Based Hardware Design of a Three-Phase Dual-Active Bridge Converter for a Bidirectional On-Board Charger," in *2020 IEEE Energy Conversion Congress and Exposition (ECCE)*, Detroit, MI, USA, 2020, pp. 850-857, doi: 10.1109/ECCE44975.2020.9236190.
- [14] Z. Yang, J. Hu, G. C. Pasupuleti and R. W. De Doncker, "Operation-Oriented Design Procedure of a Three-Phase Dual-Active Bridge Converter for a Wide Operation Range," in *2018 IEEE Energy Conversion Congress and Exposition (ECCE)*, Portland, OR, 2018, pp. 2835-2842, doi: 10.1109/ECCE.2018.8557389..
- [15] K.D. Hoang and J. Wang, J., "Design Optimization of High Frequency Transformer for Dual Active Bridge DC-DC Converter," in *XXth International Conference on Electrical Machines (ICEM)*, Marseille, France, 2012, pp. 2311-17.
- [16] F. Tourkhani and P. Viarouge, "Accurate analytical model of winding losses in round Litz wire windings," in *IEEE Transactions on Magnetics*, vol. 37, no. 1, pp. 538-543, Jan 2001, doi: 10.1109/20.914375..
- [17] C. R. Sullivan, "Optimal choice for number of strands in a litz-wire transformer winding," in *IEEE Transactions on Power Electronics*, vol. 14, no. 2, pp. 283-291, March 1999, doi: 10.1109/63.750181.
- [18] R. Bakri, X. Margueron, J. S. N. T. Magambo, P. le Moigne and N. Idir, "Power density of planar transformers designed with commercial standard cores," 2020 22nd European Conference on Power Electronics and Applications (EPE'20 ECCE Europe), 2020, pp. P.1-P.10, doi: 10.23919/EPE20ECCEEurope43536.2020.9215747
- [19] R. Petkov, "Optimum design of a high-power, high-frequency transformer," in *IEEE Transactions on Power Electronics*, vol. 11, no. 1, pp. 33-42, Jan. 1996, doi: 10.1109/63.484414
- [20] R. Wrobel, S. Ayat and J. L. Baker, "Analytical methods for estimating equivalent thermal conductivity in impregnated electrical windings formed using Litz wire," in *2017 IEEE International Electric Machines and Drives Conference (IEMDC)*, Miami, FL, 2017, pp. 1-8, doi: 10.1109/IEMDC.2017.8002003.
- [21] F. Miyashiro, N. Iwase, A. Tsuge, F. Ueno, M. Nakahashi and T. Takahashi, "High thermal conductivity aluminum nitride ceramic substrates and packages," in *IEEE Transactions on Components, Hybrids, and Manufacturing Technology*, vol. 13, no. 2, pp. 313-319, June 1990, doi: 10.1109/33.56163
- [22] P. A. Kyaw, M. Delhommais, J. Qiu, C. R. Sullivan, J. Schanen and C. Rigaud, "Thermal Modeling of Inductor and Transformer Windings Including Litz Wire," in *IEEE Transactions on Power Electronics*, vol. 35, no. 1, pp. 867-881, Jan. 2020, doi: 10.1109/TPEL.2019.2914661.
- [23] <http://www-cast3m.cea.fr/>
- [24] Mn-Zn Ferrite, Material characteristics (July 2021) TDK technical note available in <https://product.tdk.com/en/products/ferrite>.
- [25] M. de Graaf, L. Dortmans and A. Shpilman, "Mechanical reliability of ferrite cores used in inductive components," Proceedings:Electrical Electronics Insulation Conference and Electrical Manufacturing & Coil Winding Conference, 1995, pp. 485-488, doi: 10.1109/EEIC.1995.482479.
- [26] U. Soupremanien, J. -S. Ngoua-Teu, P. Sallot, C. Delafosse and G. Delette, "Soft Ferrite Material by Powder Injection Molding Process for Power Electronics," in *IEEE Transactions on Magnetics*, vol. 56, no. 12, pp. 1-7, Dec. 2020, Art no. 2000907, doi: 10.1109/TMAG.2020.3027248.